Available online at www.sciencedirect.com
ScienceDirect
Materials Research Bulletin 43 (2008) 2579–2591
Materials Research Bulletin
www.elsevier.com/locate/matresbu

Structure and lithium ion conductivity of garnet-like $Li_5La_3Sb_2O_{12}$ and $Li_6SrLa_2Sb_2O_{12}$

Ramaswamy Murugan [a,*], Werner Weppner [a,*], Peter Schmid-Beurmann [b], Venkataraman Thangadurai [c]

[a] Sensors and Solid State Ionics, Faculty of Engineering, University of Kiel, Kaiserstr. 2, D24143 Kiel, Germany
[b] Mineralogisches Institut der Westf. Wilhelms Universität Münster, Corrensstr. 24, 48149 Münster, Germany
[c] Department of Chemistry, University of Calgary, 2500 University Drive NW, Calgary, AB T2N 1N4, Canada

Received 25 April 2007; received in revised form 19 October 2007; accepted 30 October 2007
Available online 7 November 2007

Abstract

Oxides with the nominal chemical compositions $Li_5La_3Sb_2O_{12}$ and $Li_6SrLa_2Sb_2O_{12}$ were prepared by solid-state reaction. The structures were refined by the Rietveld method using powder X-ray diffraction data. The synthesis of $Li_5La_3Sb_2O_{12}$ resulted in the well known garnet-related structure plus 5 wt.% of La_2LiSbO_6 in the bulk. In contrast to that, $Li_6SrLa_2Sb_2O_{12}$ could be synthesised in single garnet-related type phase. Lithium ion conductivities of $Li_5La_3Sb_2O_{12}$ and $Li_6SrLa_2Sb_2O_{12}$ were studied by the ac impedance method. The grain-boundary contribution to the total (bulk + grain-boundary) resistance is very small and about 5 and 3% for $Li_5La_3Sb_2O_{12}$ and $Li_6SrLa_2Sb_2O_{12}$, respectively, at 24 °C and decreases further with increase in temperature. Among the investigated compounds, $Li_5La_3Sb_2O_{12}$ exhibits the highest total (bulk + grain-boundary) and bulk ionic conductivity of 7.8×10^{-6} and 8.2×10^{-6} S cm^{-1}, respectively, at 24 °C. The structural data indicate that the coupled substitution Li + Sr ⇒ La leads to a closure of the bottle neck like O–O distances of the shared edges of neighbouring Li octahedra and therefore reduces the mobility of Li ions in $Li_6SrLa_2Sb_2O_{12}$. Scanning electron microscope (SEM) images of the $Li_6SrLa_2Sb_2O_{12}$ compound revealed well crystallised large homogeneous grains (∼4.8 μm) and the grains were in good contact with the neighbouring grain, which leads to a smaller grain-boundary contribution to the total resistance.

Keywords: A. Ceramics; B. Oxides; C. Impedance spectroscopy; D. Energy storage

1. Introduction

Fast lithium ion conducting solid electrolytes have recently drawn much attention due to their potential application in all-solid-state rechargeable (secondary) batteries and also in other solid-state electrochemical devices [1–5]. Lithium ion conduction has been reported for a wide range of crystalline metal oxides and halides with different types of structure [1–5]. In general, oxide materials are believed to be superior to nonoxide materials for reasons of handling, mechanical and chemical stability [5]. Since polycrystalline materials are being used for practical applications, large

* Corresponding authors. Tel.: +49 431 8802183; fax: +49 431 8801520.
E-mail addresses: rm@ac.uni-kiel.de (R. Murugan), ww@tf.uni-kiel.de (W. Weppner), psb@uni-muenster.de (P. Schmid-Beurmann), vthangad@ucalgary.ca (V. Thangadurai).

0025-5408/$ – see front matter © 2007 Elsevier Ltd. All rights reserved.
doi:10.1016/j.materresbull.2007.10.035

grain-boundary resistances are commonly observed in addition to the bulk resistance and therefore control the total (bulk + grain-boundary) resistance of the galvanic cells. For instance, $Li_{3x}La_{(2/3)-x}\square_{(1/3)-2x}TiO_3$ ($0 < x < 0.16$) (LLT, where $\square$ represents a vacancy) exhibits a bulk conductivity of 10^{-3} S cm^{-1} and a total (bulk + grain-boundary) conductivity of 7×10^{-5} S cm^{-1} at 27 °C and $x \sim 0.1$ [6].

Recently, a novel class of fast lithium ion conducting metal oxides with the nominal chemical composition $Li_5La_3M_2O_{12}$ (M = Nb, Ta) possessing garnet-related structure has been reported from our laboratory [7,8]. Based on $Li_5La_3M_2O_{12}$, further investigations of conductivity optimisation by chemical substitutions and structural modifications were initiated. The partial replacement of divalent alkaline earth ions for a trivalent La in $Li_5La_3M_2O_{12}$ (M = Nb, Ta) extended the series of garnet-like structures by compounds with the general chemical formula of $Li_6ALa_2Nb_2O_{12}$ (A = Ca, Sr, Ba) [9] and $Li_6ALa_2Ta_2O_{12}$ (A = Sr, Ba) [10,11]. Also, partial substitution of trivalent La by monovalent K and pentavalent Nb by trivalent In in $Li_5La_3Nb_2O_{12}$ yielded new members of garnet-like structure [12]. Structure and ionic-transport properties of $Li_3Ln_3Te_2O_{12}$ (Ln = Y, Pr, Nd, Sm–Lu), reported by O'Callaghan et al., indicated that Li^+ will preferentially occupy the tetrahedral site in this series and $Li_3Nd_3Te_2O_{12}$ exhibited the maximum observed conductivity of 10^{-5} S cm^{-1} at 600 °C with an activation energy of 1.2 eV [13]. Neutron diffraction studies of the lithium garnets $Li_3Nd_3W_2O_{12}$ and $Li_5La_3M_2O_{12}$ (M = Ta, Nb and Sb) were reported recently [14,15].

Although Isasi et al. in 1991 reported the composition $Li_5Ln_3Sb_2O_{12}$ (Ln = La, Pr, Nd, Sm) [16,17], no transport measurements were carried out on these compounds. For further understanding the composition–structure–electrical conductivity relationships in the lithium containing garnet-related materials, investigations were made in this work on the structure and transport properties of $Li_5La_3Sb_2O_{12}$ and $Li_6SrLa_2Sb_2O_{12}$.

2. Experimental

2.1. Synthesis

Conventional solid-state reaction procedure was employed to prepare the title compounds. Appropriate amounts of high purity chemicals $LiNO_3$ (Sigma, >99%, 15 wt.% excess was added to compensate for the loss of lithium during annealing), $Sr(NO_3)_2$ (Riedel-de Haen, >99%), La_2O_3 (Alfa Aesar, >99.99%, pre-dried at 900 °C for 24 h) and Sb_2O_3 (Aldrich nanopowder, >99.9%) were ball-milled using zirconia balls in 2-propanol for about 12 h. After the evaporation of solvents at room temperature, the mixtures were heated to 750 °C in air for 12 h and then cooled down to room temperature. The resulting powders were ground again for another 12 h using zirconia balls in 2-propanol. After the evaporation of solvents, the powders were pressed into pellets by isostatic pressure and annealed at 950 °C in air for 48 h while the samples were covered with powder of the same mother compound to generate a high vapor pressure of the volatile components, especially to reduce the loss of Li_2O. In spite of the low sintering temperature, the density was very high and did not improve at higher temperatures.

2.2. Structural characterisation

Sintered pellets of the furnace cooled samples were cut into small coin shaped cylinders. A portion of the pellet was ground to fine powder for phase characterisation. X-ray powder diffraction patterns were recorded using a powder diffractometer (SEIFERT 3000, Germany) with Cu K_α radiation and a secondary graphite (0 0 1) monochromator with the operation conditions $U = 40$ kV and $I = 40$ mA. Qualitative phase analysis of samples was performed using the EVA-package of DiffracPlus software (BRUKER, Germany). Rietveld refinement was performed using FULLPROF SUITE 2000 [18]. For the refinements, Pseudo-Voigt Profile functions were used. Sixteen parameters were varied: 4 zero shift, 4 background parameters, scale factor, a lattice parameter, 2 peak shape parameters (degree of mixing Gauss and Lorentz in Pseudo-Voigt Profile), half width parameters w and v, asymmetry parameter, overall temperature factor B_{ov} as well as the positional parameters of oxygen (96h) x, y, z. The atomic positions and the occupancies of Li in the Wyckoff positions 24d and 96h were adopted from the neutron diffraction data of $Li_5La_3Sb_2O_{12}$ given by Cussen and Yip [14]. This was done because of the too low contribution to the scattered X-ray intensity by Li especially in the presence of heavy ions like Sb, Sr and La.

2.3. Electrical characterisation

Electrical conductivity measurements of the prepared pellets (0.17 cm in thickness and 0.91 cm in diameter of $Li_5La_3Sb_2O_{12}$ and 0.17 cm in thickness and 1.11 cm in diameter of $Li_6SrLa_2Sb_2O_{12}$) were performed in argon flow using Li-ion blocking Au-electrodes (Au paste cured at 700 °C for 1 h) in the temperature range from 24 to 300 °C by an Impedance and Gain-Phase Analyzer (HP 4192 A, Hewlett-Packard Co., Palo Alto, CA) (5 Hz–13 MHz) with an amplitude of 50 mV. Prior to each impedance measurement, the samples were equilibrated for 3–6 h at constant temperature. For each sample, the impedance was measured over two heating and cooling cycles consecutively.

2.4. Microstructural characterisation

The microstructure of the sintered pellets was observed by means of a scanning electron microscope (SEM) (PHILIPS XL 30 Series, The Netherlands). Chemical analysis of the sintered compounds and elemental mapping of the surface of the pellets were performed by energy dispersive-X-ray (EDX) equipment operated at 20 kV.

2.5. Thermal analysis

Thermogravimetric (TG) and Differential Thermal Analysis (DTA) (STA 409 C/CD NETZSCH, Germany) data for the prepared sample were collected under argon atmosphere in the temperature range 20–900–20 °C with a heating/cooling rate of 2 °C min^{-1} and isothermally keeping the temperature at 900 °C for 1 h.

3. Results and discussion

3.1. Structural characterisation

The result of the qualitative and quantitative phase analysis of the samples is given in Table 1. The synthesis of the sample $Li_5La_3Sb_2O_{12}$ resulted in the well known garnet-type compound $Li_5La_3Sb_2O_{12}$ (PDF-80-1251) [17] plus a second phase, which could be identified as La_2LiSbO_6 (PDF 81-0839) [19]. Quantitative phase analysis resulted in an amount of 5 wt.% of La_2LiSbO_6 in the bulk. In contrast to that, $Li_6SrLa_2Sb_2O_{12}$ could be synthesised as single garnet type phase. Due to the coupled substitution $Sr^{2+} + Li^{+} \Leftrightarrow La^{3+}$, the *a* lattice parameter increases from 12.8566(18) to 12.8933(3) Å. The results of the Rietveld refinements of our samples are presented in Figs. 1 and 2 and Table 2.

Recently, using neutron diffraction, it was shown that the structure of the garnets $Li_5La_3M_2O_{12}$ (M = Nb, Ta) can be better described in the symmetry space group $Ia\bar{3}d$ rather than in the space groups $I2_13$ or $Ia\bar{3}$ which were applied formerly [13–15]. Our X-ray powder diffraction data collected for the Li–(La,Sr)–Sb-samples could be indexed in the above-mentioned space group $Ia\bar{3}d$. No Bragg peaks could be detected that violated the systematic absences associated with this space group. The X-ray diffraction patterns of both compounds indicated the presence of a cubic cell with the same systematic absences. Therefore, as starting parameters for the Rietveld refinement of the Sb-compounds $Li_5La_3Sb_2O_{12}$ and $Li_6SrLa_2Sb_2O_{12}$ we used the structural data for $Li_5La_3Sb_2O_{12}$ given by Cussen and Yip [14]. In case of the Sr containing compound, this model was also applied as we assumed that this ion substitutes La on its crystallographic site. In order to model the contribution of the Li ions we used the Li-positional parameters and the occupancies given by Cussen and Yip [14] for $Li_5La_3Sb_2O_{12}$. In case of our X-ray diffractions we could not confirm the findings of O'Callaghan et al. [13] concerning sensitivity of the X-ray diffraction data with regard to the lithium cations in the presence of heavy atoms in $Li_5Ln_3Te_2O_{12}$. This may be due to the higher scattering power of Sb compared to Te. Therefore, in order to model the Li distribution of $Li_6SrLa_2Sb_2O_{12}$, we assumed that the additional Li ion per formula compared to $Li_5La_3Sb_2O_{12}$ enters exclusively the less occupied octahedral Li2-oc (96h) positions (see Table 2).

Table 1
Results of qualitative phase analysis and lattice parameters of $Li_5La_3Sb_2O_{12}$ and $Li_6SrLa_2Sb_2O_{12}$ compounds at room temperature

Composition	Phases detected	Lattice parameter
$Li_5La_3Sb_2O_{12}$	Garnet type $Li_5La_3Sb_2O_{12}$ PDF-80-1251 + 5 wt.% La_2LiSbO_6 PDF 81-0839	12.8566(18) Å
$Li_6SrLa_2Sb_2O_{12}$	Garnet type $Li_6SrLa_2Sb_2O_{12}$	12.8933(3) Å

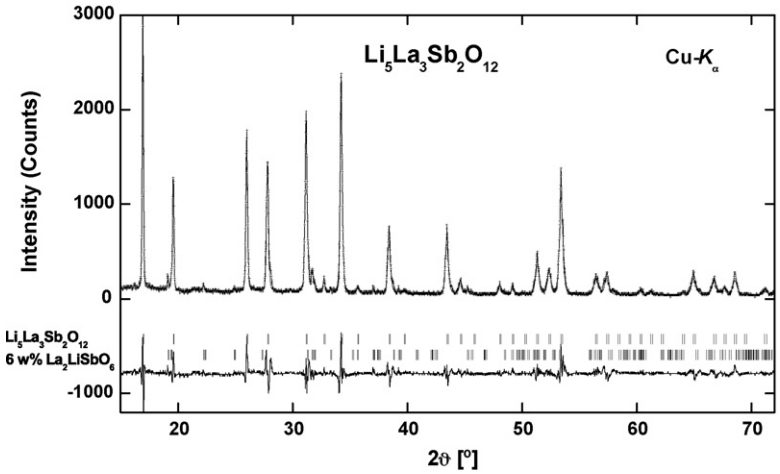

Fig. 1. Observed (dots), calculated (line), allowed Bragg peak positions for the garnet phase (upper markers) and La_2LiSbO_6 (intermediate markers) and difference X-ray powder diffraction pattern (lower marker) collected from $Li_5La_3Sb_2O_{12}$ at room temperature.

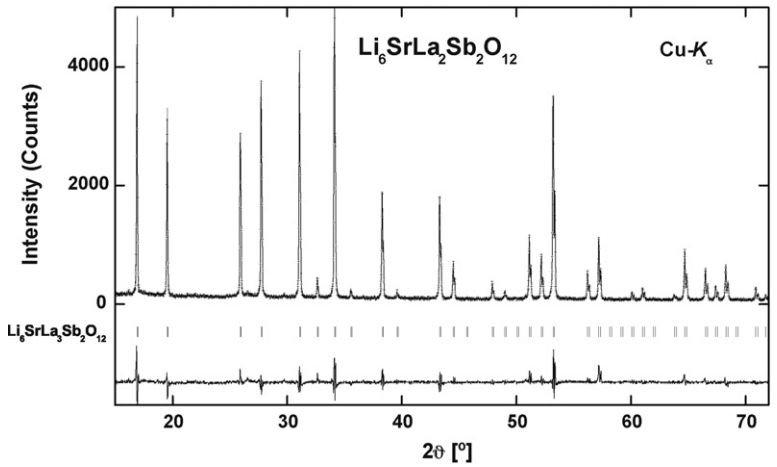

Fig. 2. Observed (dots), calculated (line), allowed Bragg peak positions for the garnet phase (upper marker) and difference X-ray powder diffraction pattern (lower marker) collected from $Li_6SrLa_2Sb_2O_{12}$ at room temperature.

3.2. Electrical properties

The combined impedance and modulus spectroscopy has been demonstrated to be a useful technique for analysing the ac resistance behaviour of polycrystalline solid electrolytes, which enables separation of grain-boundary phenomena from the bulk behaviour [20]. The modulus formalism is based on the concept of electric modulus M^* and is defined as the reciprocal of the complex dielectric permittivity (ε^*)

$$M^* = \left(\frac{1}{\varepsilon^*}\right) = M' + jM'' \tag{1}$$

The real (M') and imaginary (M'') parts of the complex electric modulus were obtained from real (ε') and imaginary (ε'') parts of the complex dielectric constant using the relations

$$M' = \frac{\varepsilon'}{(\varepsilon'^2 + \varepsilon''^2)} \quad \text{and} \quad M'' = \frac{\varepsilon''}{(\varepsilon'^2 + \varepsilon''^2)} \tag{2}$$

Typical impedance and spectroscopic plots of the imaginary components of the impedance Z'' and electric modulus M'' against log(frequency) obtained at 24 °C are shown in Fig. 3a and b for $Li_5La_3Sb_2O_{12}$ and in Fig. 4a and b for

Table 2
Structural parameters of Li–(La,Sr)–(Sb)–O garnets from Rietveld refinement of X-ray powder diffractions at room temperature (space group $Ia\bar{3}d$)

	Site	$Li_5La_3Sb_2O_{12}$ [14]	$Li_5La_3Sb_2O_{12}$	$Li_6SrLa_2Sb_2O_{12}$
Sb *x*, *y*, *z*	24c	1/8, 0, 1/4	1/8, 0, 1/4	1/8, 0, 1/4
(La, Sr) *x*, *y*, *z*	16a	0, 0, 0	0, 0, 0	0, 0, 0
Li1-t *x*, *y*, *z*	24d	1/4, 7/8 0	1/4, 7/8 0	1/4, 7/8 0
Occupancy		*0.793*(*8*)	*0.793*(*8*)	*0.793*(*8*)
Li2-oc *x*	96h	*0.107*(*1*)	*0.107*(*1*)	*0.107*(*1*)
y		*0.6676*(*8*)	*0.6676*(*8*)	*0.6676*(*8*)
z		*0.6171*(*8*)	*0.6171*(*8*)	*0.6171*(*8*)
Occupancy		*0.218*(*2*)	*0.218*(*2*)	*0.218*+0.0833*
O *x*	96h	*0.27994*(*4*)	0.2827(23)	0.2820(10)
y		*0.10666*(*5*)	0.1080(23)	0.1055(10)
z		*0.19932*(*5*)	0.1971(25)	0.2031(12)
a [Å]		12.8518(3)	12.8566(18)	12.8933(3)
$B_{overall}$			0.50(16)	0.78(8)
R_p/R_{wp}			14.7/19.5	10.2/12.9
GOF/R_{exp}			2.1/14.0	1.7/12.7
R_{Bragg}			7.6	6.7

Note: Data in italics are taken from Cussen and Yip [14]. Site occupancies for oxygen were set to unity. *: In order to model the Li distribution in $Li_6SrLa_2Sb_2O_{12}$ it was assumed that the additional Li enters completely the Li (96h) position.

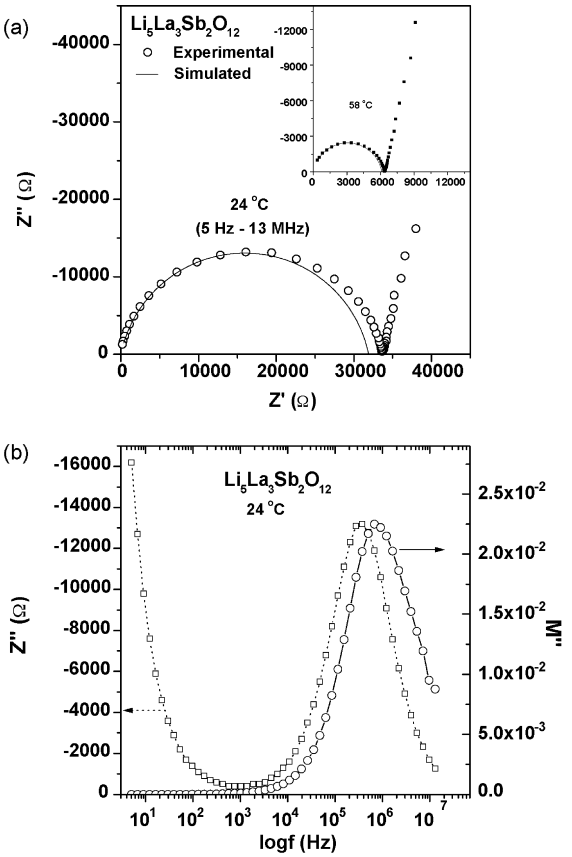

Fig. 3. (a) ac impedance and (b) spectroscopic plots of the imaginary components of the impedance Z'' and electric modulus M'' against log(frequency) obtained at 24 °C for $Li_5La_3Sb_2O_{12}$. The impedance plot of $Li_5La_3Sb_2O_{12}$ obtained at 58 °C is shown as inset in (a). The line connecting the experimental impedance data points have been fitted using the EQUIVALENT program [23] with an equivalent circuit consisting of parallel resistance–capacitance for the bulk contribution.

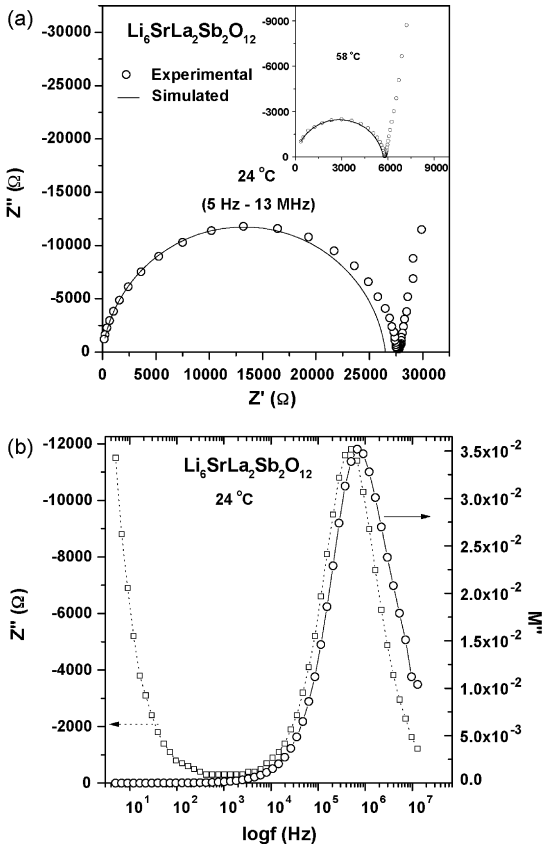

Fig. 4. (a) ac impedance and (b) spectroscopic plots of the imaginary components of the impedance Z'' and electric modulus M'' against log(frequency) obtained at 24 °C for $Li_6SrLa_2Sb_2O_{12}$. The impedance plot of $Li_6SrLa_2Sb_2O_{12}$ obtained at 58 °C is shown as inset in (a). The line connecting the experimental impedance data points have been fitted using the EQUIVALENT program [23] with an equivalent circuit consisting of parallel resistance–capacitance for the bulk contribution.

$Li_6SrLa_2Sb_2O_{12}$, respectively. The impedance plots shown in Figs. 3a and 4a indicate nearly a single semicircle and a tail at the low frequency side. The tail at the low frequency side in case of ionically blocking electrodes is an initial indication that the investigated material is ionic in nature [20–22]. Furthermore, preliminary Hebb-Wagner measurements resulted in very low currents as compared to values expected from impedance measurements. The current showed a plateau which indicates n-type minority charge carriers.

To understand the microstructure of the pellet and to determine whether the total resistance of the pellet represented the bulk resistance or a contribution of the grain-boundary, the impedance data obtained at 24 °C for $Li_5La_3Sb_2O_{12}$ and $Li_6SrLa_2Sb_2O_{12}$ are plotted as imaginary part of the impedance Z'' and electrical modulus M'' against log(frequency), as shown in Figs. 3b and 4b, respectively. The impedance plot emphasises the most resistive elements of the sample while the modulus plot highlights those elements with the smallest capacitance since the peak height of M'' is proportional to $1/C$ for that element [20]. Since the capacitance corresponding to grain-boundary response is relatively large compared to the bulk response, the large peak in M'' corresponds to bulk response. However, in the present work, both plots of Z'' and M'' vs. log f (Figs. 3b and 4b) contain a single peak in the same frequency regime demonstrating that this semicircle seems to be mainly related to just one dielectric effect, probably the bulk response and accordingly the grain-boundary contribution is being small.

The solid line in Figs. 3a and 4a represents fitted data with an equivalent circuit consisting of a parallel resistance–capacitance for bulk contribution using the EQUIVALENT program [23]. The bulk resistance, grain-boundary resistance, bulk conductivity, total conductivity (bulk + grain-boundary) and ratio between grain-boundary resistance and total (bulk + grain-boundary) resistance obtained at 24 and 58 °C for both $Li_5La_3Sb_2O_{12}$ and $Li_6SrLa_2Sb_2O_{12}$ are summarised in Table 3. It is interesting to note that the grain-boundary contribution to the total

Table 3
Impedance data of $Li_5La_3Sb_2O_{12}$ and $Li_6SrLa_2Sb_2O_{12}$ in argon

Compound	Temperature (°C)	R_b† (ς)	R_{gb}† (ς)	σ_{bulk} (S cm^{-1})	σ_{total} (S cm^{-1})	$R_{gb}/R_b + R_{gb}$
$Li_5La_3Sb_2O_{12}$	24	31902	1698	8.2×10^{-6}	7.8×10^{-6}	0.05
	58	6128	234	4.3×10^{-5}	4.1×10^{-5}	0.03
$Li_6SrLa_2Sb_2O_{12}$	24	26503	1097	6.6×10^{-6}	6.3×10^{-6}	0.03
	58	5696	99	3.1×10^{-5}	3.0×10^{-5}	0.02

† R_b = bulk resistance, R_{gb} = grain-boundary resistance.

(bulk + grain-boundary) resistance is very small and about 5 and 3% for $Li_5La_3Sb_2O_{12}$ and $Li_6SrLa_2Sb_2O_{12}$, respectively, at 24 °C and decreases further with increase of temperature. The grain-boundary contribution to the total electrical conductivity is very small for $Li_5La_3Sb_2O_{12}$ compared to the related $Li_5La_3M_2O_{12}$ (M= Nb, Ta) [7] systems. As previously, we observed that the alkaline earth ion substitution for La and simultaneous addition of Li for charge compensation in the parent compound $Li_5La_3M_2O_{12}$ (M = Nb, Ta) [9–11] reduces the grain-boundary contribution. Similarly, here in the present work, the strontium substituted $Li_6SrLa_2Sb_2O_{12}$ exhibits a slight reduction in the grain-boundary contribution to the total resistance compared to $Li_5La_3Sb_2O_{12}$.

The bulk (8.2×10^{-6} S cm^{-1}) and total (7.8×10^{-6} S cm^{-1}) conductivity obtained for $Li_5La_3Sb_2O_{12}$ is slightly higher than the bulk (6.6×10^{-6} S cm^{-1}) and total (6.3×10^{-6} S cm^{-1}) conductivity of $Li_6SrLa_2Sb_2O_{12}$ at 24 °C. The slight reduction in the bulk as well as total conductivity with the substitution of strontium for lanthanum with a simultaneous addition of lithium in $Li_5La_3Sb_2O_{12}$ is similar to the observation made with the Nb containing garnet $Li_5La_3Nb_2O_{12}$ [9]. At higher temperature (above 75 °C), it is difficult to separate bulk and grain-boundary contributions accurately; accordingly, we have consistently indicated the total (bulk + grain-boundary) electrical conductivity over the investigated temperature range.

The Arrhenius plots for the total (bulk + grain-boundary) electrical conductivity of $Li_5La_3Sb_2O_{12}$ and $Li_6SrLa_2Sb_2O_{12}$ are shown in Figs. 5 and 6, respectively. The data obtained from heating and cooling cycles follow the same line, which implies that the investigated garnet-like structure compounds are thermally stable without any phase transition in the investigated temperature range between room temperature and 300 °C. The activation energies (E_a) for the ionic conductivity were determined from the Arrhenius plots employing the equation:

$$\sigma T = A \exp\left[\frac{-Ea}{kT}\right], \tag{1}$$

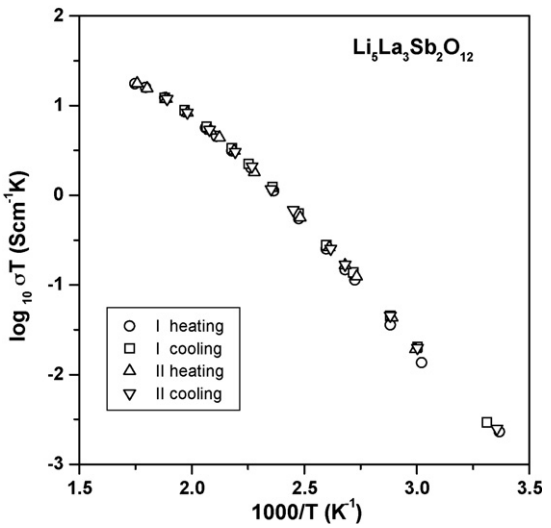

Fig. 5. Arrhenius plots for the total (bulk + grain-boundary) lithium ion conductivity of $Li_5La_3Sb_2O_{12}$. The data were obtained from two consecutive heating and cooling runs in argon and follow the same line.

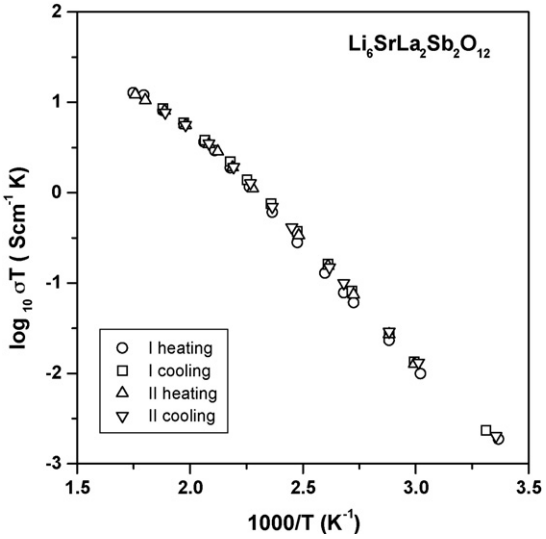

Fig. 6. Arrhenius plots of the total (bulk + grain-boundary) lithium ion conductivity of $Li_6SrLa_2Sb_2O_{12}$. The data were obtained from two heating and cooling cycles consecutively in argon and follow the same line.

where A is the pre-exponential parameter, k is Boltzmann's constant and T is the absolute temperature. The bending observed at high temperatures is an experimental artifact due to the low resistance of the samples. The total resistance of the metallic leads and the sample reach more and more a constant value with increasing temperature. Using thicker pellets, the bending shifts to higher temperatures compared to thin pellet measurements.

The activation energies for the total lithium ion conductivity of $Li_5La_3Sb_2O_{12}$ and $Li_6SrLa_2Sb_2O_{12}$ are 0.51 and 0.54 eV, respectively, and are comparable to other garnet-related fast lithium ion conductors such as $Li_5La_3Ta_2O_{12}$ (0.56 eV) [7], $Li_5La_3Nb_2O_{12}$ (0.55 eV) [12], $Li_6CaLa_2Nb_2O_{12}$ (0.55 eV) [9], $Li_6SrLa_2Nb_2O_{12}$ (0.50 eV) [9], $Li_6BaLa_2Nb_2O_{12}$ (0.44 eV) [9], $Li_6SrLa_2Ta_2O_{12}$ (0.50 eV) [10], $Li_6BaLa_2Ta_2O_{12}$ (0.40 eV) [10], $Li_{5.5}La_3Nb_{1.75}In_{0.25}O_{12}$ (0.49 eV) [12] and $Li_{5.5}La_{2.75}K_{0.25}Nb_2O_{12}$ (0.53 eV) [12].

The variation of electrical modulus M'' against log(frequency) at different temperatures provides information related to the charge transport processes. The electrical modulus M'' against log(frequency) observed at several temperatures for the $Li_6SrLa_2Sb_2O_{12}$ compound is shown in Fig. 7. The peak frequency f_m in Fig. 7 represents the most

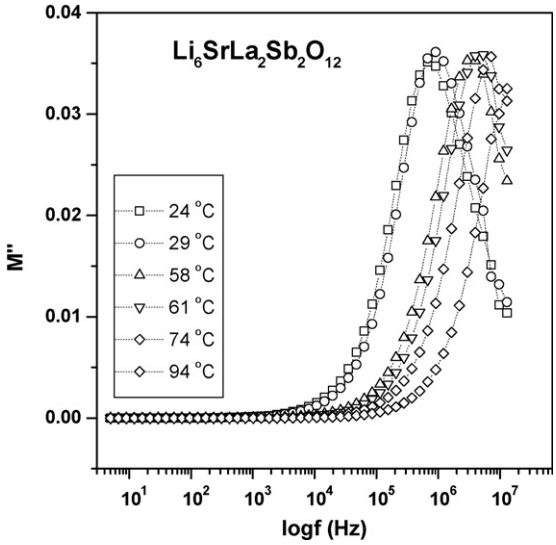

Fig. 7. Spectroscopic plots of the imaginary components of the electric modulus M'' against log(frequency) obtained at various temperatures for $Li_6SrLa_2Sb_2O_{12}$.

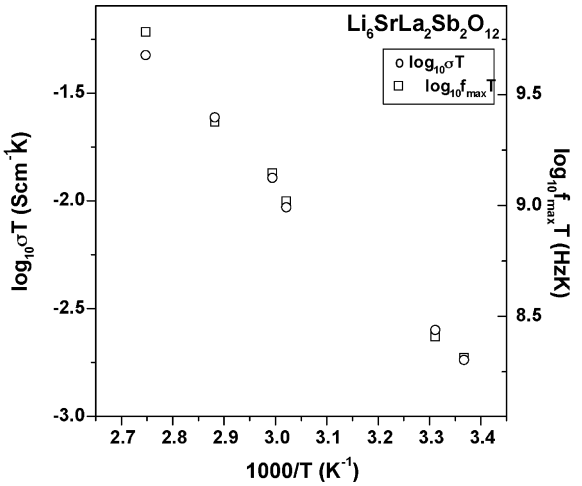

Fig. 8. Arrhenius representation for $Li_6SrLa_2Sb_2O_{12}$ of $\log(\sigma T)$ (open circles) vs. $1000/T$ and $\log(f_mT)$ (open squares) vs. $1000/T$ obtained in the temperature range from 24 to 94 °C.

probable conductivity relaxation frequency from the relation $f_m\tau_m = 1$, where τ_m is the characteristic relaxation time. The peak frequency f_m shifts towards higher frequencies with increasing temperature.

A better information on the bulk conduction properties may be obtained from Arrhenius plots of the frequency (f_m) at the modulus peak maximum (M''_{max}) [24]. The activation energy (E_a) was determined from

$$f_mT = f_0 \exp\left[\frac{-Ea}{kT}\right], \tag{3}$$

where f_0 is the pre-exponential parameter of the relaxation frequency.

For comparison, the Arrhenius representations of $\log(\sigma T)$ and $\log(f_mT)$ vs. $1000/T$ for $Li_6SrLa_2Sb_2O_{12}$ obtained over the temperature range from 24 to 94 °C are shown in Fig. 8. The activation energy derived from the slope of $\log(f_mT)$ vs. $1000/T$ corresponds to bulk conductivity, i.e., the long-range translational motion of Li^+ ions. The activation energies obtained from $\log(\sigma T)$ vs. $1000/T$ and $\log(f_mT)$ vs. $1000/T$ are 0.49 and 0.43 eV, respectively. The similarity in the activation energy again confirms that the observed electrical conductivity is mainly due to the bulk response and the grain-boundary contribution is being very small. Fig. 9 shows the normalised imaginary part of the modulus (M'') vs. normalised $\log(f)$ for $Li_6SrLa_2Sb_2O_{12}$ obtained for three different temperatures. The overlap of the

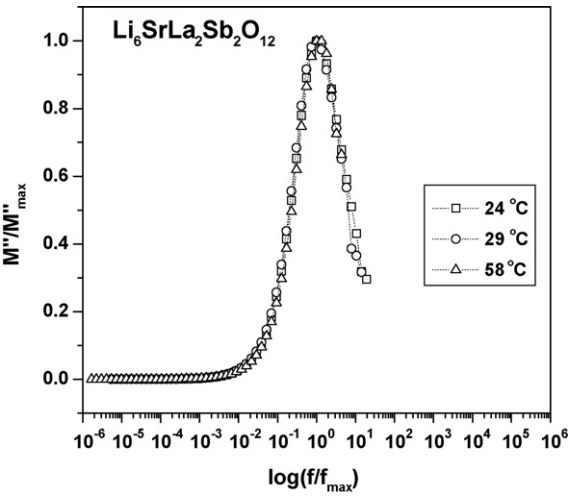

Fig. 9. Normalised imaginary part of the modulus (M''/M''_{max}) vs. normalised $\log(f/f_{max})$ for $Li_6SrLa_2Sb_2O_{12}$ obtained for three different temperatures.

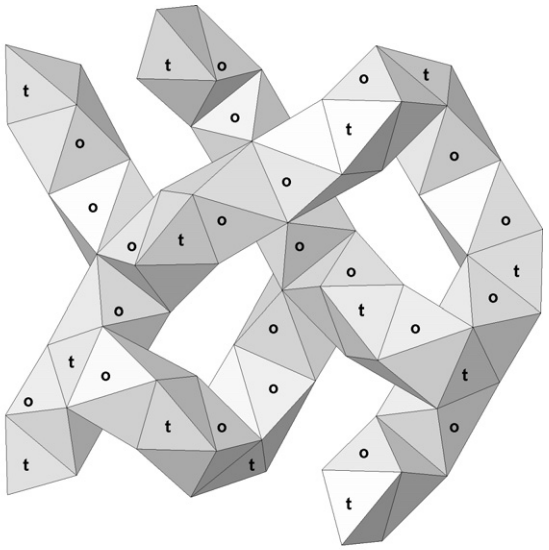

Fig. 10. The three-dimensional network of Li-polyhedra in Li-garnets according to the model of Cussen and Yip [14]. t: tetrahedral site; o: octahedral site.

curves indicates that the electrical conductivity relaxation processes are temperature independent. The full width at half maximum (FWHM) is about 1.49 decades and is slightly higher than 1.14 decades expected for a Debye peak [24].

3.3. Lithium ion diffusion pathway

Fig. 10 shows a sketch of the Li-polyhedra in the garnet structure which are interconnected by faces and edges and form a three-dimensional network of channels in which Li-diffusion may occur. The heart of this system is a cluster of four symmetrically equivalent octahedra with a tetrahedral void (the fourth octahedron being omitted in Fig. 10 in order to recognise better the tetrahedral position in the void). Such clusters act as crossings in the above-mentioned three-dimensional network. According to the model of Cussen and Yip [14], about 79.3% of the tetrahedral positions are occupied by Li (Li1-t in 24d) in $Li_5La_3Sb_2O_{12}$ garnet. In case of the octahedra, the Li ions occupy a position which is slightly shifted from the centres of the neighbouring octahedra (Li2-oc in 96h). The occupancy of this octahedral position is 21.8% respectively [14]. The Li octahedra are linked by shared edges and the shortest cation separation is correlated with the longest O–O distances facilitating Li hopping between these sites. Therefore, it can be assumed that Li mobility arises from hopping between the octahedral sites, which show a minor Li occupancy in contrast to the tetrahedral positions (Li1-t, 24d). In Fig. 11a and b we compare the O–O distances in our compounds $Li_5La_3Sb_2O_{12}$ and $Li_6SrLa_2Sb_2O_{12}$. In $Li_5La_3Sb_2O_{12}$, the O–O distances of the sharing edges between neighbouring octahedra are 3.22 and 3.07 Å, whereas in $Li_6SrLa_2Sb_2O_{12}$, which contains one more Li per formula, the O–O distances amount to 3.19 and 2.98 Å. Therefore, we can state that substitution of Li + Sr for one La decreases the O–O distances and should therefore reduce the mobility of Li ions in the structure.

3.4. Microstructural characterisation

Preliminary work on the influence of the microstructure on the ionic conductivity of $Li_5La_3Sb_2O_{12}$ and $Li_6SrLa_2Sb_2O_{12}$ prepared under the same sintering conditions was carried out and SEM images are shown in Fig. 12. It is seen that the $Li_5La_3Sb_2O_{12}$ compound (Fig. 12a) revealed better densification compared to $Li_6SrLa_2Sb_2O_{12}$ (Fig. 12b). Usually, a large grain-boundary resistance is commonly observed in polycrystalline materials in addition to the bulk resistance. However, in the present investigation, both $Li_5La_3Sb_2O_{12}$ and $Li_6SrLa_2Sb_2O_{12}$ exhibit a very small grain-boundary resistance contribution at room temperature, which decreases further with increasing temperature. The

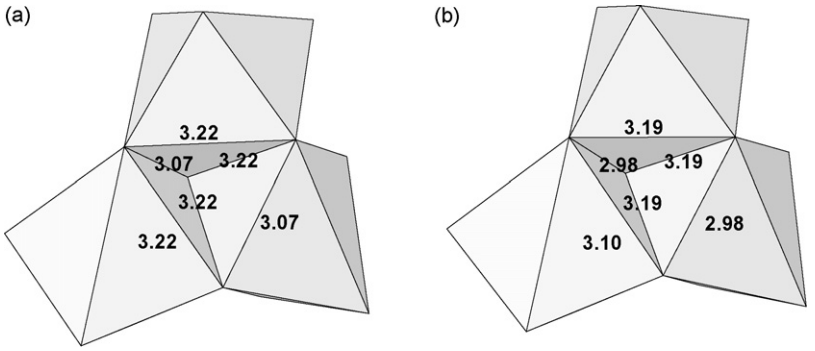

Fig. 11. Li2- and Li3-octahedra and O–O distances (Å) in (a) $Li_5La_3Sb_2O_{12}$ and (b) $Li_6SrLa_2Sb_2O_{12}$.

SEM images of the compounds $Li_5La_3Sb_2O_{12}$ and $Li_6SrLa_2Sb_2O_{12}$ revealed that most of the grains were in good contact with the neighbours. Particularly, the magnified SEM image of $Li_6SrLa_2Sb_2O_{12}$, shown in Fig. 12c, clearly revealed well crystallised large homogeneous grains (~4.8 μm) and large contact areas of the grains with the neighbouring grains. Chemical analysis of the sintered compounds and elemental mapping of the surface of the pellets performed by energy dispersive X-ray equipment showed uniform distribution of the elemental constituents. The intergranular regions in these compounds appear to be composed of the same composition and structure as the bulk and this could lead to low resistance for the current pathways at the contact of the grains.

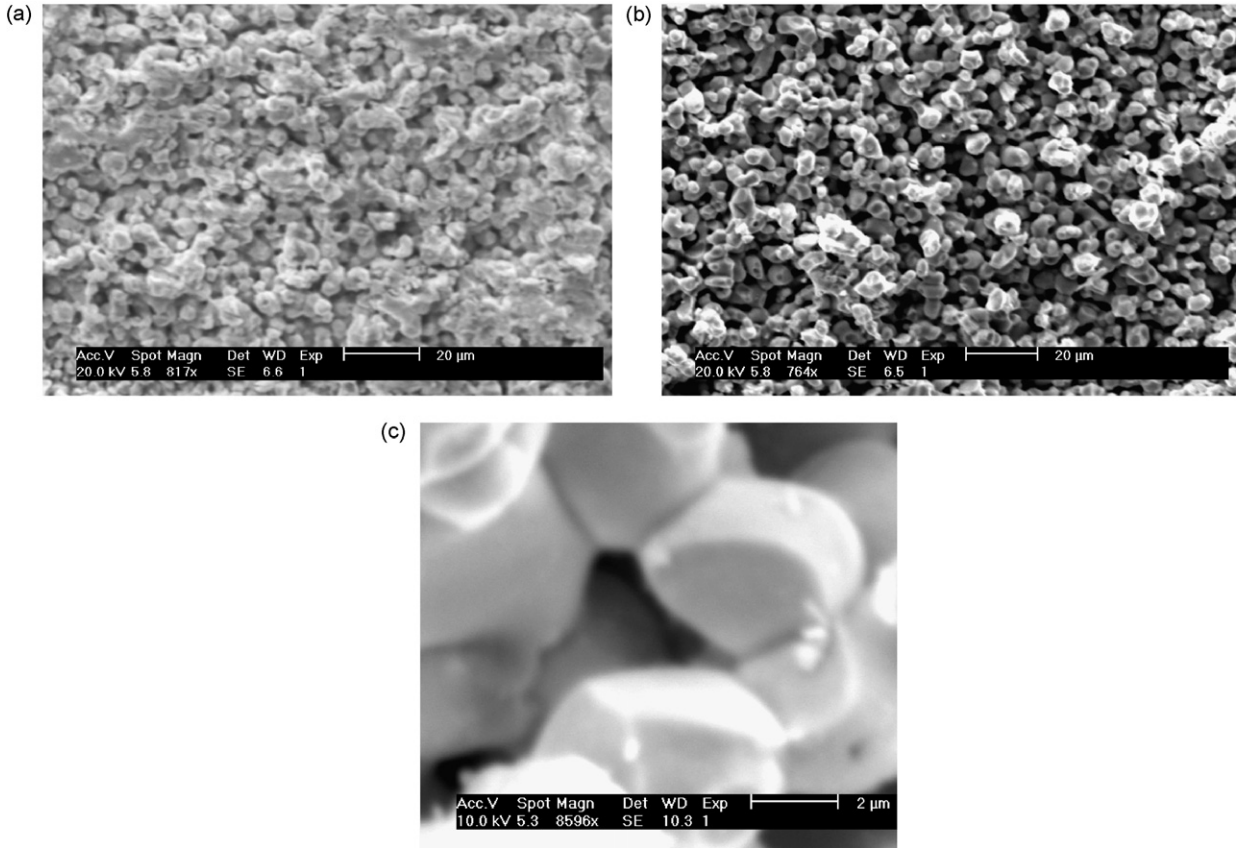

Fig. 12. SEM images of (a) $Li_5La_3Sb_2O_{12}$, (b) $Li_6SrLa_2Sb_2O_{12}$ and (c) magnified SEM image of $Li_6SrLa_2Sb_2O_{12}$.

3.5. Thermal analysis

The thermal stability of the investigated compounds was confirmed by Thermogravimetric and Differential Thermal Analysis measurements. The TG–DTA data of the prepared sample collected in an argon atmosphere revealed no significant change in mass and no detectable phase transition in both the heating and cooling process over the temperature range from 20 to 900 °C.

4. Conclusions

Fast lithium ion conductors $Li_5La_3Sb_2O_{12}$ and $Li_6SrLa_2Sb_2O_{12}$ with garnet-related structure were prepared by solid-state reaction. The synthesis of $Li_5La_3Sb_2O_{12}$ resulted in the garnet-related type structure with 5 wt.% of La_2LiSbO_6 as second phase. In contrast to that, $Li_6SrLa_2Sb_2O_{12}$ could be synthesised in a single garnet-related type phase. The structures were refined by Rietveld method using powder X-ray diffraction data. Among the investigated compounds, both bulk and total conductivity of $Li_5La_3Sb_2O_{12}$ are slightly higher than the bulk and total conductivity of $Li_6SrLa_2Sb_2O_{12}$ at 24 °C. At this stage of investigation, we can assume from our structural data that the coupled substitution Li + Sr ⇒ La definitely leads to a closure of the bottle neck like O–O distances of the shared edges of neighbouring Li octahedra and therefore reduces the mobility of Li ions in $Li_6SrLa_2Sb_2O_{12}$. The grain-boundary contribution to the total (bulk + grain-boundary) resistance is very small for both $Li_5La_3Sb_2O_{12}$ and $Li_6SrLa_2Sb_2O_{12}$ at 24 °C and decreases further with increasing temperature. The scanning electron microscope image of the $Li_6SrLa_2Sb_2O_{12}$ compound revealed well crystallised large homogeneous grains (∼4.8 μm) and the grains were in large contact with the neighbouring ones, which leads to a smaller grain-boundary contribution to the total resistance.

Acknowledgement

The authors would like to thank the German Science Foundation (DFG grant WE 684/11-1) for financial support.

Appendix A. Supplementary data

Supplementary data associated with this article can be found, in the online version, at doi:10.1016/j.materresbull.2007.10.035.

References

[1] A.D. Robertson, A.R. West, A.G. Ritchie, Solid State Ionics 104 (1997) 1.
[2] (a) G.Y. Adachi, N. Imanaka, H. Aono, Adv. Mater. 8 (1996) 127;
(b) T. Kudo, in: P.J. Gellings, H.J.M. Bouwmeester (Eds.), The CRC Handbook of Solid State Electrochemistry, CRC Press, London, 1997, p. 195.
[3] C. Julien, G.A. Nazri, Solid State Batteries: Materials Design and Optimization, Kluwer Academic Publications, Boston, 1994.
[4] H. Aono, N. Imanaka, G.Y. Adachi, Acc. Chem. Res. 27 (1991) 265.
[5] J.T.S. Irvine, A.R. West, in: T. Takahashi (Ed.), High Conductivity Solid Ionic Conductors, Recent Trends and Applications, World Scientific, Singapore, 1989, p. 201.
[6] (a) Y. Inaguma, C. Liquan, M. Itoh, T. Nakamura, T. Uchida, H. Ikuta, W. Wakihara, Solid State Commun. 86 (1993) 689;
(b) H. Kawai, J. Kuwano, J. Electrochem. Soc. 141 (1994) L78;
(c) O. Bohnke, C. Bohnke, J.L. Fourquet, Solid State Ionics 91 (1996) 21.
[7] V. Thangadurai, H. Kaack, W. Weppner, J. Am. Ceram. Soc. 86 (2003) 437.
[8] V. Thangadurai, S. Adams, W. Weppner, Chem. Mater. 16 (2004) 2998.
[9] V. Thangadurai, W. Weppner, J. Am. Ceram. Soc. 88 (2005) 411.
[10] V. Thangadurai, W. Weppner, Adv. Funct. Mater. 15 (2005) 107.
[11] V. Thangadurai, W. Weppner, J. Power Sources 142 (2005) 339.
[12] V. Thangadurai, W. Weppner, J. Solid State Chem. 179 (2006) 974.
[13] M.P. O'Callaghan, D.R. Lynham, E.J. Cussen, G.Z. Chen, Chem. Mater. 18 (2006) 4681.
[14] E.J. Cussen, Th.W.S. Yip, J. Solid State Chem. 180 (2007) 1832.
[15] E.J. Cussen, Chem. Commun. (2006) 412.
[16] J. Isasi, M.L. Veiga, R. Saez-Puche, A. Jereze, C. Pico, J. Alloys Compd. 177 (1991) 251.
[17] J. Isasi, M.L. Veiga, A. Jereze, C. Pico, J. Less-Common Met. 167 (1991) 381.

[18] J. Rodriguez-Carvajal, Full Prof Suite, Lab. de Léon Brillouin (CEA-CNRS) CEA/Saclay, France, 2000.
[19] M.L. Lopez, M.L. Veiga, J. Rodriguez-Carvajal, F. Fernandez, A. Jerez, C. Pico, Mater. Res. Bull. 27 (647) (1992) 647.
[20] J.T.S. Irvine, D.C. Sinclair, A.R. West, Adv. Mater. 2 (1990) 132.
[21] V. Thangadurai, R.A. Huggins, W. Weppner, J. Power Sources 108 (2002) 64.
[22] J.E. Bauerle, J. Phys. Chem. Solids 30 (2657) (1969) 2657.
[23] B.A. Boukamp, "Equivalent Circuit," Version 4.55, 1997, Faculty of Chemical Technology, University of Twente, 7500 AE Enschede (The Netherlands. Reports No: CT88/265/128/CT89/214/128, May 1989).
[24] E.R. Losilla, M.A.G. Aranda, S. Bruque, M.A. Paris, J. Sanz, A.R. West, Chem. Mater. 10 (1998) 665.